Energetic and Conformational Contributions to the Stability of Okazaki Fragments†

Ana Maria Soto,‡ William H. Gmeiner,§ and Luis A. Marky*,‡,||,⊥

Department of Pharmaceutical Sciences, Department of Biochemistry and Molecular Biology, and Eppley Institute for Cancer Research, University of Nebraska Medical Center, 986025 Nebraska Medical Center, Omaha, Nebraska 68198-6025, and Department of Biochemistry, Wake Forest University, Medical Center Boulevard, Winston-Salem, North Carolina 27157-1016

Received February 21, 2002; Revised Manuscript Received April 4, 2002

ABSTRACT: A combination of spectroscopic and calorimetric techniques was used to determine complete thermodynamic profiles accompanying the folding of a model Okazaki fragment with sequence 5′-r(gagga)d-(ATCTTTG)-3′/5′-d(CAAAGATTCCTC)-3′ and control DNA (with and without thymidine substitutions for uridine), RNA, and hybrid duplexes. Circular dichroism spectroscopy indicated that all DNA duplexes are in the B conformation, the RNA and hybrid duplexes are in the A conformation, and the Okazaki fragment exhibits a spectrum between the A and B conformations. Ultraviolet and differential scanning calorimetry melting experiments reveal that all duplexes unfold in two-state transitions with thermal stabilities that follow the order RNA > OKA > DNA (with thymidines) > hybrids > DNA (with uridines). The dependence of the transition temperature on salt concentration yielded counterion releases in the following order: DNA (with thymidines) > RNA > DNA (with uridines) > OKA > hybrids. Thus, Okazaki fragments have a conformation and charge density between those of its components DNA and hybrid segments. However, the presence of the RNA−DNA/DNA junction confers on them higher stabilities than their component hybrid and DNA segments. The binding of intercalators to an Okazaki hairpin of sequence 5′-r(gc)d(GCU5GCGC)-3′ and to its control DNA hairpin has also been studied. The results show that the binding of intercalators to Okazaki fragments is accompanied with higher heats and lower binding affinities, compared with DNA duplexes. This suggests that the presence of an RNA/DNA junction yields a larger surface contact to interact with the phenanthroline ring of the intercalators, which may lead to a larger disruption of the flexible flanking bases of the junction. The overall results suggest that the presence of this junction stabilizes Okazaki fragments and provides a structural feature that can be exploited in the design of drugs to specifically target these molecules.

Okazaki fragments appear as intermediates during the replication of the DNA "lagging strand", the strand that is elongated in a discontinuous fashion. The 3′−5′ polarity of this strand dictates that its replication proceeds by joining short DNA fragments. This discontinuous replication involves the unwinding of the parental strands, synthesis of an RNA primer, extension of a DNA chain in the 5′−3′ direction, removal of the RNA primer, filling of the gaps between the DNA pieces, and joining of the DNA pieces (*1*). The duplex intermediates that exist before removal of the RNA primers are called Okazaki fragments, which consist of a 5′-RNA−DNA-3′ segment base paired to the DNA parent strand. Because the frequency of DNA replication is much higher for cancer cells than for normal cells, Okazaki fragments provide potential targets for the design of anticancer drugs (*2*, *3*).

RNase H1 is the enzyme involved in the removal of the RNA primers of Okazaki fragments. Although this enzyme can cleave RNA/DNA hybrids in an unspecific fashion, it has been recently found that it also contains a junction RNase activity that recognizes and cleaves RNA at the RNA−DNA/DNA junction (hereafter called the RNA−DNA junction) of Okazaki fragments (*4*). This enzyme is able to recognize a distinct feature in the structure of Okazaki fragments. Therefore, it is reasonable to think that this RNA−DNA junction could be exploited in the development of drugs that target Okazaki fragments. Moreover, theoretical modeling of an A−B junction (*5*) and high-resolution NMR structures (*2*, *6*−*8*) have suggested the presence of a helix bend at the RNA−DNA junction of model Okazaki fragments. This structural feature can be exploited in the design of drugs to specifically target Okazaki fragments, and some constrained bis(distamycin)s have been found to bind with different affinities to Okazaki fragments than to DNA duplexes (*9*, *10*). However, in the development of drugs that target these structures, it is important to have a clear idea on the stability and physical properties of these molecules. To improve our understanding of Okazaki fragments, what is needed are clear answers to the following questions. Does the presence of a helical bend affect their stability? Is it possible to differentiate these fragments from their DNA, RNA, and DNA/RNA hybrid counterparts? What is the conformation at the RNA−

† Supported by NIH GM42223 (L.A.M.), NIH NCI CA60612 and P30 CA12197 (W.H.G.), and a Blanche Widaman Fellowship (A.M.S.) from UNMC.

* Author to whom correspondence should be addressed [telephone (402) 559-4628; fax (402) 559-9543; e-mail lmarky@unmc.edu].

‡ Department of Pharmaceutical Sciences, University of Nebraska Medical Center.

§ Department of Biochemistry, Wake Forest University.

|| Department of Biochemistry and Molecular Biology, University of Nebraska Medical Center.

⊥ Eppley Institute for Cancer Research, University of Nebraska Medical Center.

10.1021/bi025715o CCC: $22.00
Published on Web 05/01/2002

DNA junction? Is it possible to differentiate Okazaki fragments from DNA duplexes using simple drugs?

In this work we have used a combination of optical and calorimetric techniques to determine the stability of a model Okazaki fragment with a sequence derived from the genome of simian virus 40 (SV40).[1] We compared its stability with that of control DNA (with and without thymine substitutions with uridines), RNA, and DNA/RNA hybrid duplexes with the same sequence. Our results show that the presence of the RNA−DNA junction in Okazaki fragments confers them with intermediate stability, conformation, and charge density parameter with regard to those of their component fragments, DNA, RNA, and hybrid segments. We have also compared the binding of intercalators to an intramolecular Okazaki fragment and to a DNA hairpin of the same sequence. Our results show that intercalators bind to Okazaki fragments with reduced binding affinities and higher exothermic heats, compared to DNA duplexes. These results illustrate the different base stacking interactions that exist at the RNA−DNA junction of Okazaki fragments. Furthermore, the results suggest that it may be possible to exploit these structural differences and to design intercalators that specifically recognize Okazaki fragments.

MATERIALS AND METHODS

Materials. All oligonucleotides were synthesized by the Core Synthetic Facility of the Eppley Research Institute at the University of Nebraska Medical Center, HPLC purified, and desalted by column chromatography. The concentration of the oligomer solutions was determined at 260 nm and 80 °C using the following molar extinction coefficients, in mM^{-1} cm^{-1} of strands: 5′-r(caaag)d(ATTCCTC)-3′, 118; 5′-d(CAAAGATTCCTC)-3′, 120.4; 5′-d(GAGGAATCTTTG)-3′, 126.5; 5′-r(caaagauuccuc)-3′, 124.5; 5′-r(gaggaaucuuug)-3′, 129.1; 5′-d(CAAAGAUUCCUC)-3′, 123.9; 5′-d(GAGGAAUCUUUG)-3′, 133; 5′-d(GCGCUUUUUGCGC)-3′, 116; and 5′-r(gc)d(GCUUUUUGCGC)-3′, 115.9. These values were calculated by extrapolation of the tabulated values of the dimers and monomer bases (*11*) at 25 °C to high temperatures, using procedures reported earlier (*12*). Buffer solutions consisted of 10 mM sodium cacodylate, 100 mM sodium chloride, adjusted to pH 7.0, or 10 mM sodium phosphate, adjusted to pH 7.0. Except for the last two sequences, which are designed to form intramolecular structures, appropriate mixing of complementary single strands resulted in 1:1 DNA, RNA, hybrid, or Okazaki fragment duplexes. All duplexes investigated and their corresponding designations are shown in Chart 1. Ethidium bromide (EB) and propidium iodide (PI) were purchased from Sigma and Aldrich, respectively, and were used without further purification. The concentration of EB was determined at 480 nm using a molar extinction coefficient (ϵ) of 5850 M^{-1} cm^{-1} (*13*), whereas the concentration of PI was obtained at 496 nm using an ϵ of 5900 M^{-1} cm^{-1} (*14*).

Circular Dichroism (CD). Evaluation of the conformation of each duplex was obtained by simple inspection of their CD spectrum. These spectra were obtained on a Jasco J-710 spectropolarimeter, using a 10 mm quartz cuvette. All spectra were collected at room temperature, between 200 and 400 nm, using a wavelength step of 0.5 nm. All spectra represent the average of at least two scans.

Chart 1: Sequence of Duplexes and Hairpins[a]

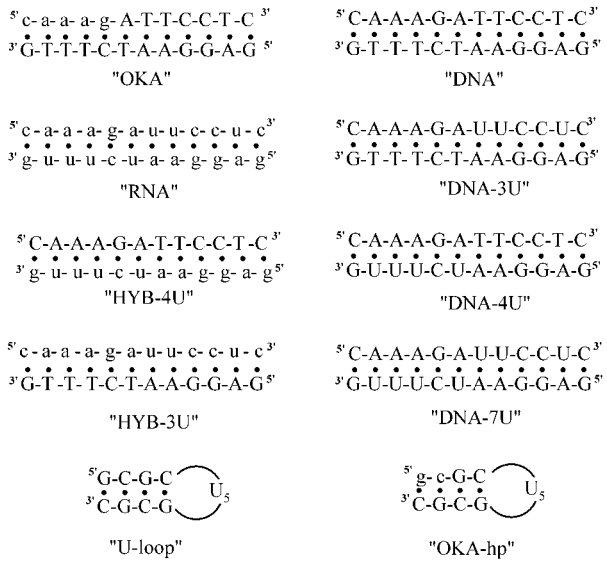

[a] RNA bases are shown in lower cases; DNA bases are in upper cases.

Temperature-Dependent UV Spectroscopy (UV Melts). Absorbance versus temperature profiles (melting curves) for each duplex were measured at 260 nm with a thermoelectrically controlled Aviv 14-DS spectrophotometer and as a function of strand and salt concentration. The temperature was scanned at a heating rate of ~0.6 °C/min. These melting curves allow us to measure transition temperatures, T_M, which are the midpoint temperatures of the order−disorder transition of the duplexes, van't Hoff enthalpies, ΔH_{shape} and ΔH_{vH}, using a two-state transition approximation as reported previously (*15*), and the thermodynamic release of counterions, Δn_{Na^+}.

Differential Scanning Calorimetry (DSC). Excess heat capacity as a function of temperature melts for the helix−coil transition of each oligomer was measured with a Microcal MC-2 differential scanning calorimeter (Northampton, MA). Two cells, the sample cell containing 1.6 mL of oligomer solution and the reference cell filled with the same volume of buffer solution, were heated from 10 to 100 °C at a heating rate of 0.75 °C/min. Analysis of the resulting thermograms, using procedures described previously, yields standard thermodynamic profiles (ΔH_{cal}, ΔS_{cal}, and ΔG°_{cal}) and model-dependent van't Hoff enthalpies, ΔH_{vH}, for the transition of each hairpin.

Isothermal Titration Calorimetry. Binding heats for the interaction of EB and PI with each hairpin were measured directly by isothermal titration calorimety using the Omega calorimeter from Microcal Inc. The instrument was calibrated by means of known standard electrical pulses. The titrant solution, placed in a 250 μL syringe, was 40-fold more concentrated than the hairpin solution in the reaction cell. Rotation of the syringe paddle at 400 rpm ensured complete mixing of both reactants. The heat of mixing, following the injection of 5 μL of titrant solution, was calculated from the area of the peak, corrected by dilution heat of the ligand, and normalized by the concentration of added titrant. Analysis of the calorimetric binding isotherm, normalized

[1] Abbreviations: SV40, simian virus 40; EB, ethidium bromide; PI, propidium iodide; DSC, differential scanning calorimetry; CD, circular dichroism; ITC, isothermal titration calorimetry.

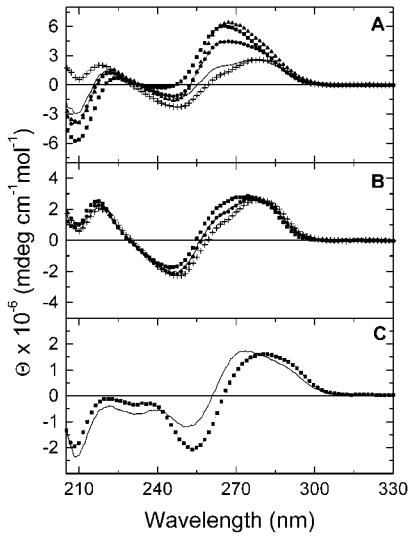

FIGURE 1: CD spectra of duplexes in 10 mM sodium cacodylate, 100 mM NaCl, pH 7.0, and of hairpins in 10 mM sodium phosphate, pH 7: (A) RNA (■), HYB−3U (▲), HYB−4U (●), OKA (−), and DNA (+); (B) DNA−7U (■), DNA−3U (−), HYB−4U (●), and DNA (+); (C) U-loop (■) and OKA-hp (−).

heats as a function of the added titrant, using Origin (v 2.9), allows us to obtain binding enthalpies, ΔH_b, binding affinities (K_b), and the overall stoichiometry of the complexes (n). Alternatively, ΔH_b can be obtained from the heats under nonsaturating conditions (initial injections).

Job Plots. The stoichiometry of the intercalator/hairpin complexes was determined primarily by titration calorimetry experiments. Alternatively, the stoichiometries of the EB/hairpin complexes were measured spectroscopically, using the method of continuous variation. A hairpin solution is titrated with ligand at a constant total concentration of hairpin and ligand. The experimental observable is the change in absorbance at 480 and 540 nm as a function of the mole fraction of hairpin. Two linear dependences are obtained, at low and high molar fractions, which intercept at a mole fraction value that corresponds to the stoichiometry of the complex.

RESULTS

Circular Dichroism. The CD spectrum of each duplex is shown in Figure 1. All DNA duplexes exhibit a CD spectrum characteristic of right-handed helices in the B conformation, with similar magnitudes of the positive (∼278 nm) and negative (∼245 nm) bands. The hybrid and RNA duplexes exhibit the spectra of the A conformation, with a large positive band (∼266 nm) and a very small negative band (∼245 nm). The Okazaki fragment exhibits a spectrum that is between the A and B conformations, with a larger magnitude of the positive band relative to the negative band. This positive band is considerably reduced relative to the positive band of the A conformation, as shown in Figure 1.

UV Melts. UV melting experiments were used to characterize the helix−coil transition of each duplex and hairpin (data not shown). Above 10 °C all curves follow the characteristic sigmoidal behavior for the unfolding of a nucleic acid duplex. UV melts at different total strand concentrations (shown in Figure 2) were conducted to determine the T_M dependence on strand concentration and van't Hoff enthalpies, ΔH_{vH}. Model-dependent van't Hoff enthalpies were determined in two different ways: from the shape of the resulting melting curves, according to the equation $\Delta H_{shape} = 6RT_M^2\ \partial\alpha/\partial T$ (*15*), and from the slopes of plots of $1/T_M$ versus $\ln(C_T/4)$, according to the equation for non-self-complementary duplexes: $1/T_M = R/\Delta H_{vH}\ \ln(C_T/4) + \Delta S/\Delta H_{vH}$ (*15*). Both methods yielded similar van't Hoff enthalpies (data not shown), and only the ΔH_{vH} values from the latter plots are shown in Table 1. As the thermal stability of the duplexes depends on its concentration, plots of the T_M as a function of strand concentration were also used to obtain the T_M corresponding to a total strand concentration of 100 μM. The T_M dependences on strand concentration for the hairpin unfolding are shown in Figure 2C. Over a 70-fold concentration range, the T_M values of the U-loop and OKA-hp are independent of strand concentration, confirming the formation of intramolecular hairpins. We used the resulting melting curves and the equation $\Delta H_{shape} = 4RT_M^2\ \partial\alpha/\partial T$ (*15*) to calculate ΔH_{shape} values of −38 kcal/mol (U-loop) and −36 kcal/mol (OKA-hp) for the folding of these hairpins.

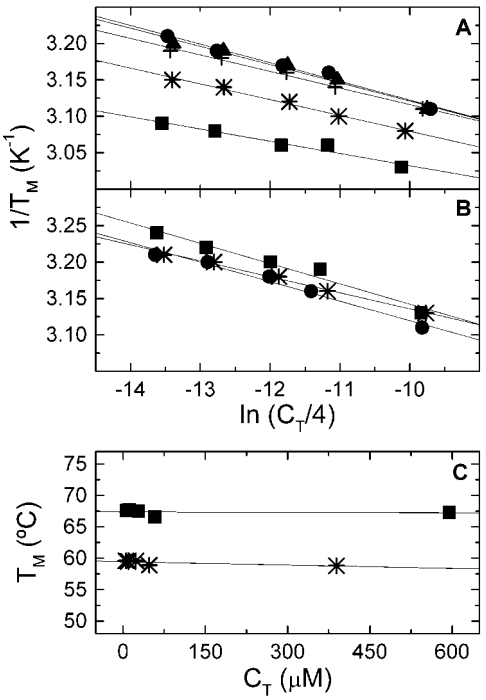

FIGURE 2: T_M dependence on total strand concentration for duplexes and hairpins: (A) RNA (■), HYB−3U (▲), HYB−4U (●), OKA (∗), and DNA (+); (B) DNA−7U (■), DNA−3U (∗), and HYB−4U (●); (C) U-loop (■) and OKA-hp (∗).

Differential Scanning Calorimetry. The DSC melting curves of each oligonucleotide are shown in Figure 3. The thermodynamic profiles for the folding of each duplex at 5 °C were determined from DSC experiments and are summarized in Table 1. The ΔH_{cal} and ΔS_{cal} parameters were measured directly using the equations $\Delta H_{cal} = \int \Delta C_p^a\ dT$ and $\Delta S_{cal} = \int (\Delta C_p^a/T)\ dT$, where ΔC_p^a is the anomolous heat capacity during the unfolding process. It is assumed there are no heat capacity effects between the initial and final states, that is, $\Delta C_p = 0$. The free energy at 5 °C, ΔG°_{278}, is obtained from the Gibbs equation: $\Delta G^\circ_{278} = \Delta H_{cal} - T\Delta S_{cal}$. In addition, van't Hoff enthalpies were calculated from the shape of the calorimetric curves (data not shown). These enthalpies are similar to the ones obtained from the

Table 1: Thermodynamic Profiles for the Formation of Duplexes and Hairpins at 5 °C[a]

	T_M (°C)	$\Delta G°_{278}$ (kcal/mol)	ΔH_{cal} (kcal/mol)	ΔH_{vH} (kcal/mol)	$T\Delta S_{cal}$ (kcal/mol)	$\partial T_M/\partial \ln[Na^+]$ (°C)	Δn_{Na^+} per P_i
				Duplexes			
OKA	50.3	−12.4	−88.4	−87	−76.0	6.07	0.129
DNA	46.6	−11.1	−85.3	−87	−74.2	6.94	0.146
RNA	55.8	−18.3	−118.6	−112	−100.3	5.13	0.142
HYB−4U	45.6	−10.4	−81.6	−78	−71.2	5.77	0.116
HYB−3U	45.8	−10.4	−81.6	−76	−71.2	5.52	0.111
DNA−7U	43.3	−9.3	−77.2	−73	−67.9	6.85	0.132
DNA−4U	45.5	−10.4	−81.7	−78	−71.3	6.91	0.139
DNA−3U	44.5	−10.2	−82.0	−84	−71.8	6.69	0.137
				Hairpins			
U-loop	67.3	−6.8	−36.9	−36	−30.1	2.06	0.062
OKA-hp	58.8	−6.2	−38.4	−36	−32.2	2.28	0.073
T-loop[b]	69.2	−7.4	−39.2	−38	−31.8		0.095

[a] Experiments were conducted in 10 mM sodium cacodylate buffer, 100 mM NaCl, pH 7 (duplexes), or 10 mM sodium phosphate buffer, pH 7 (hairpins). T_M values are normalized for a total strand concentration of 100 μM (duplexes). ΔH_{vH} values are obtained from the T_M dependence on strand concentration (duplexes) or from the shape of calorimetric melting curves (hairpins). Δn_{Na^+} are calculated per phosphate, considering 22 phosphates/mol of duplex and 6 phosphates/mol of hairpin. T_M values are within 0.5 °C, ΔH_{cal} within 3%, ΔG and $T\Delta S$ within 5%, ΔH_{vH} within 10%, and Δn_{Na^+} within 6%. [b] Values for T-loop were taken from refs *18* and *22*.

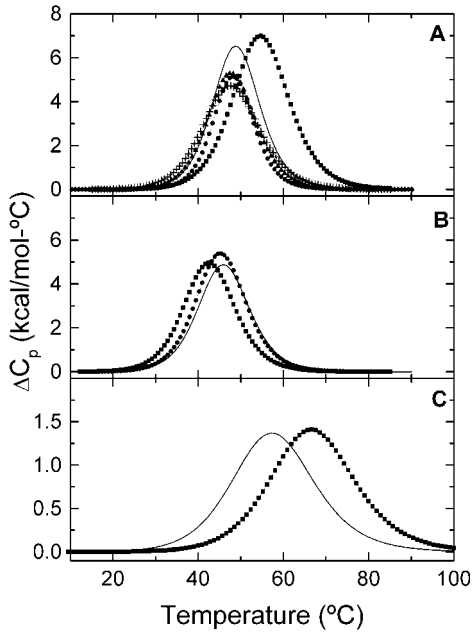

FIGURE 3: Typical DSC curves in 10 mM sodium cacodylate buffer, pH 7 (duplexes), or 10 mM sodium phosphate buffer, pH 7 (hairpins), at total strand concentrations of 100 μM: (A) RNA (■), HYB−3U (▲), HYB−4U (●), OKA (−), and DNA (+); (B) DNA−7U (■), DNA−3U (−), and HYB−4U (●); (C) U-loop (■) and OKA-hp (−).

T_M dependence on strand concentration. A comparison of the van't Hoff enthalpies with the calorimetric enthalpies is shown in Table 1; $\Delta H_{vH}/\Delta H_{cal}$ ratios of 0.93−1.02 are obtained. This shows that all molecules, duplexes and hairpins, melt in two-state transitions; that is, the transitions occur in an all-or-none fashion without the presence of intermediate states. Inspection of Table 1 indicates that the folding of each duplex at 5 °C is accompanied by favorable free energy terms resulting from the characteristic compensation of a favorable enthalpy and unfavorable entropy terms. In general, these favorable enthalpy terms correspond mainly to the formation of base-pair stacking interactions, whereas the unfavorable entropy terms arise from contributions of the unfavorable association of two strands and the uptake of both counterions and water molecules. The magnitudes of the T_M (at 100 μM strand concentration) and $\Delta G°_{278}$ (extent of exergonicity) are in the following order: RNA (55.8 °C, −18.3 kcal/mol) > OKA > DNA > Hyb3U ∼ Hyb4U ∼ DNA4U > DNA3U > DNA7U (43.3 °C, −9.3 kcal/mol). Thus, OKA exhibits a T_M and a thermodynamic profile that are between those of the RNA and DNA duplexes, whereas the DNA duplexes with uridines are the least stable ones. The T_M of the DNA duplex is higher than that of the hybrid duplexes, and their thermodynamic profiles follow the same trend. These results are in good agreement with previous studies in which hybrid duplexes containing an equal mix of purine−pyrimidine bases were less stable than their DNA and RNA counterparts (*16*, *17*). However, this observation may not be true for all mixed purine−pyrimidine sequences as their relative stabilities may depend on the actual sequence. The DNA duplexes containing uridines are less stable than DNA; moreover, DNA−7U is the least stable, indicating that these substitutions decrease the stability of DNA. Furthermore, as the number of uridines increases, the ΔH_{cal} decreases, suggesting that the presence of uridine decreases base stacking contributions.

In the case of the hairpins, the U-loop is more thermally stable than OKA-hp but their thermodynamic profiles at 5 °C are similar. These results contrast with those observed in the duplex systems in which OKA is more stable than DNA.

Thermodynamic Release of Counterions. UV melting curves at several salt concentrations and the T_M dependence on salt concentration are shown in Figure 4. The thermodynamic release of counterions, Δn_{Na^+}, is determined from the equation $\Delta n_{Na^+} = -1.11(\Delta H_{cal}/RT_M^2)\,\partial T_M/\partial \ln[Na^+]$ (*18*), where the $\partial T_M/\partial \ln[Na^+]$ term corresponds to the slope of T_M versus $\ln[Na^+]$ plots, the term in parentheses is obtained in DSC melting experiments, R is the universal gas constant, and 1.11 is a proportionality constant for converting concentrations into ionic activities. The resulting Δn_{Na^+} values are shown in Table 1. We obtained Δn_{Na^+} values ranging from 0.111 to 0.146 mol of Na^+/phosphate (duplexes) and from 0.062 to 0.073 mol of Na^+/phosphate (hairpins) considering only the helical phosphates of these molecules (22 and 6, respectively). The magnitudes of Δn_{Na^+} for the

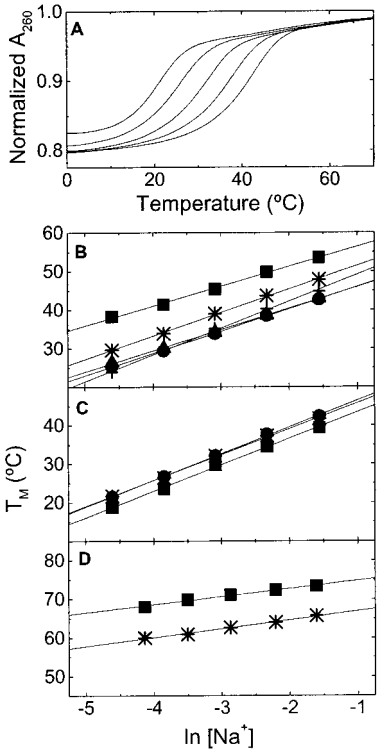

FIGURE 4: UV melting curves of oligonucleotides, at constant strand concentration of 5 μM, as a function of salt concentration in 10 mM sodium cacodylate buffer, pH 7 (duplexes), or 10 mM sodium phosphate buffer, pH 7 (hairpins): (A) typical melting curves over a NaCl concentration range of 10−210 mM; (B) dependence of T_M on salt concentration for RNA (■), HYB−3U (▲), HYB−4U (●), OKA (∗), and DNA (+); (C) DNA−7U (■), DNA−3U (∗), and HYB−4U (●); (D) U-loop (■) and OKA-hp (∗).

set of duplexes are in the following order: DNA > RNA > DNA−4U > DNA−3U > DNA−7U > OKA > HYB−3U > HYB−4. The overall differences are small, but it is clear that OKA exhibits a counterion uptake between those of DNA and hybrid duplexes, as shown in Table 1. These results are in contrast with the profiles obtained in the hairpin set in which the DNA hairpin exhibits a lower release of counterions when compared to the Okazaki hairpin.

Isothermal Titration Calorimetry. A representative ITC titration for the interaction of PI with OKA-hp, and the corresponding binding isotherm, are shown in Figure 5. The thermodynamic profiles for the interaction of EB and PI with U-loop and OKA-hp are calculated from fitting the ITC binding isotherms. These profiles are summarized in Table 2. The interactions of these hairpins with EB and PI exhibit exothermic heats, binding affinities of the order of 10^5-10^6, and multiple site binding stoichiometries. The stem of these hairpins is designed to contain only one binding site for intercalators. Thus, the stoichiometries of three ligands per hairpin suggest the presence of additional binding sites in the uridine loops. The interaction of these intercalators with the stem of OKA-hp is more exothermic than with U-loop, whereas the binding affinities follow the opposite trend, that is, they are higher for the interaction with U-loop.

Job Plots. The binding stoichiometries of the EB/hairpin complexes were also determined in continuous variation experiments. Job plots for the interaction of EB with U-loop and OKA-hp are shown in Figure 6. The interception of the lines in each plot takes place at a mole fraction of 0.67, which

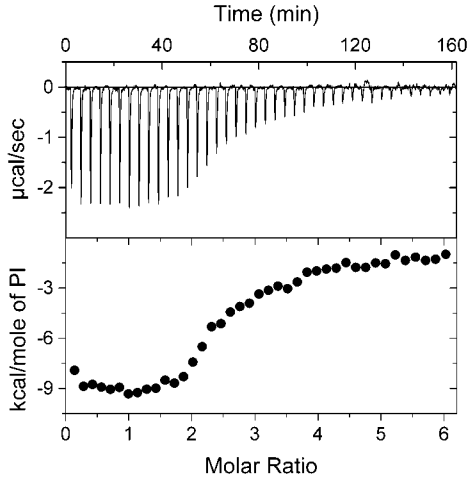

FIGURE 5: Typical calorimetric titration (A) and binding isotherm (B). Data shown correspond to the titration of 1.4 mL of a 40 μM OKA-hp solution with 5 μL aliquots of a 1.6 mM solution of propidium iodide.

Table 2: Thermodynamic Profiles for the Interaction of Ethidium and Propidium with Hairpins[a]

hairpin	site	*n* (mol of ligand/ mol of DNA)	ΔH_b (kcal/mol)	$K \times 10^{-5}$ (M^{-1})
		Ethidium		
U-loop	stem	1	−9.2	20
	loop	2	−11.2	0.4
OKA-hp	stem	1.1	−12.7	2.7
	loop	1.1	−15.0	0.4
T-loop[a]	stem	0.9	−9.8	17
	loop	1.8	−8.9	0.7
		Propidium		
U-loop	stem	1	−6.8	34.5
	loop	2.1	−13.0	0.6
OKA-hp	stem	0.9	−8.8	28.6
	loop	1.9	−10.9	0.6
T-loop[b]	stem	1	−8.3	40
	loop	2	−7.9	0.4

[a] All experiments were conducted at 20 °C, in 10 mM sodium phosphate buffer, pH 7. ΔH_b values are within 3%, K_b within 50%, and *n* within 10%. [b] Values for T-loop were taken from refs *18* and *22*.

corresponds to a stoichiometry of 2 ligands/hairpin molecule. These stoichiometries confirm the multiple sites observed in ITC, although the stoichiometries from ITC are greater (3 ligands/hairpin). This apparent discrepancy may reflect the weaker binding affinity of the loops sites, which are accompanied by negligible absorbance changes (*19*). Alternatively, the spectroscopic properties of the complex with three bound ligands may differ slightly from those of the complex with two ligands.

DISCUSSION

Duplex Design. The sequence of the Okazaki fragment was derived from the SV40 genome. This virus has been extensively studied (*20*, *21*). The selection of this fragment may allow us to understand how the stability of Okazaki fragments affects their biological function. Furthermore, the structure of this fragment has been solved using NMR techniques (*2*, *6*, *22*), allowing us to correlate the energetics and structural features of these structures. The length of these duplexes constitutes a full helical turn, and their sequence

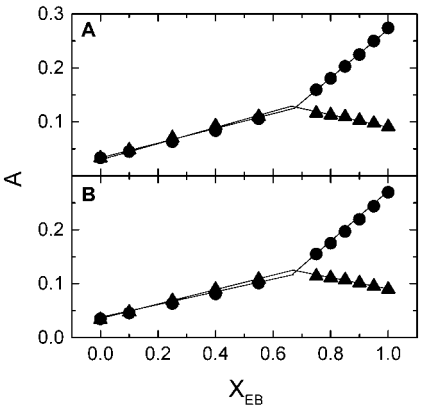

FIGURE 6: Continuous variation experiments (Job plots) for the determination of complex stoichiometries in 10 mM sodium phosphate buffer, pH 7 and 25 °C. Each panel corresponds to the Job plot resulting from the interaction of ethidium with U-loop (A) and OKA-hp (B). Wavelengths used were 480 nm (●) and 540 nm (▲). Total concentration (ethidium plus hairpin) was kept constant at 40 μM throughout the experiments.

has been carefully designed to avoid the formation of intramolecular structures. On the other hand, the sequence of the hairpins is designed to allow the formation of intramolecular structures that melt at convenient temperatures. EB and PI have a binding preference of 5′Pyr-3′Pur (*23*, *24*), and therefore the stem sequence 5′-GCGC-3′ contains only one binding site for these intercalators, which, in the case of OKA-hp, is right at the RNA−DNA junction. This design allows us to directly probe if this junction can be exploited for targeting purposes using intercalators.

Circular Dichroism. All DNA duplexes exhibit a CD spectrum characteristic of right-handed helices in the B conformation, whereas the hybrid and RNA duplexes exhibit spectra of the A conformation. On the basis of NMR studies, hybrid duplexes have been proposed to be in the H conformation in which the sugars in the RNA bases are C2′ endo, whereas the sugars in the DNA bases are C3′ endo (*6*−*8*, *25*, *26*). However, the CD spectra of these structures are similar to the CD spectrum of RNA (*25*, *27*, *28*). Furthermore, it has been observed that when hybrid duplexes are composed of mixed purine−pyrimidine sequences, as in this case, their spectra have greater similarity to that of pure RNA (*17*). The CD spectra of the duplex and hairpin Okazaki fragments appear to have contributions of both A and B conformations. This is consistent with existing NMR data, which show that the residues at the DNA duplex segment remain close to the B conformation, whereas the residues in the hybrid segment remain in the H conformation (*6*−*8*, *26*, *29*). The DNA sugar puckerings of the residues at the RNA−DNA junction are between A and B forms (*6*). The sugar puckering of the RNA residue adopts the A-form geometry (*6*).

Comparison of the spectra of "DNA" with the DNA duplexes containing uridines (Figure 1B) indicates that the presence of uridine shifts the spectra toward smaller wavelengths. This may indicate that the absence of the C5 methyl groups results in a different electron delocalization around the aromatic bases.

Thermodynamic Profiles. The thermodynamic profiles shown in Table 1 indicate that the higher stability of the RNA duplex arises from its more favorable enthalpic contribution. It has been suggested that duplexes in the A conformation contain intra- as well as interstrand stacking interactions, whereas the stacking of duplexes in the B conformation is limited to intrastrand stacking interactions (*30*). The increased base overlap observed in A helices arises from the unique combination of a small rotation per nucleotide, a positive base tilt, and a right helical screw sense (*30*) that gives rise to a larger enthalpy contribution. The hybrid duplexes have smaller enthalpy contribution and lower stability. This is in contrast with their CD spectra, which is typical for duplexes in the A conformation, suggesting similar stabilities for hybrids and RNA duplexes. However, NMR studies have shown that hybrid duplexes are neither in the A nor in the B conformation (*25*, *27*, *28*). Instead, their RNA segment is closer to the A form and their DNA segment is intermediate between A and B forms (*7*, *27*). This structural arrangement may not allow interstrand overlap. Moreover, base pairing between the RNA and DNA strands may also decrease their intrastrand stacking interactions. RNA strands contain uridines, whereas DNA strands contain thymidines. To determine if the presence of uridine bases contributes to the stability of RNA duplexes, we studied three additional DNA duplexes in which we replaced T for U in the top strand (DNA−3U), in the bottom strand (DNA−4U), or in both strands (DNA−7U). These three duplexes exhibit smaller enthalpies and T_M values compared with the nonsubstituted DNA. The effect seems to increase as the number of uridines increases, although it is not exactly additive. The results demonstrate that the increased stability of the RNA duplex does not arise from the presence of uridines in its sequence and that the methyl groups of thymidine bases stabilize DNA duplexes. The stabilizing effect of the thymidine methyl groups may arise from both electronic and hydrophobic effects. The electron donor properties of the methyl group may alter the aromaticity of the pyrimidine base to which it is attached, whereas its interaction with neighboring atomic groups or solvent molecules may result in favorable van der Waals interactions. The proposed effect of methyl groups in the aromatic properties thymidine is consistent with the observed shift in the CD spectra of uridine-containing DNA duplexes. The Okazaki fragment exhibits a T_M and thermodynamic profiles between those of the DNA and RNA duplexes. As OKA fragments are composed of a DNA and a DNA/RNA hybrid segment, one would expect their stabilities to be between those of DNA and hybrid duplexes. The increased stability of OKA may be attributed to the presence of an RNA−DNA junction. NMR studies have shown that the adenines in either strand of the DNA segment closest to the junction exhibit increased base stacking interactions (*2*). Furthermore, the presence of a helical bend of 18° at the RNA−DNA junction may result in increased stacking interactions in one of the strands, immobilizing structural water (*31*−*33*), which has a stabilizing effect. Bending will contribute a higher T_M due to an increase of hydrophobic hydration at this site, as has been shown for static bends (*34*).

For comparative purposes and to further analyze the effect of the loops in the stability of these hairpins, the results of a similar DNA hairpin containing thymidine loops (*19*, *23*) (T-loop) are also shown in Table 1. The stability of these hairpins follows the order T-loop > U-loop > OKA-hp; therefore, the presence of additional methyl groups in the

loops (with higher structural hydration) has a stabilizing effect. This reverse order of stability relative to the duplexes may arise from the smaller size of the Okazaki hairpin. The junction is exactly in the middle of the stem of OKA-hp, expanding two base pairs in the middle, leaving only one base pair at either end to restore the normal helicity of the DNA and hybrid segments. Thus, the decreased stability of OKA-hp may reflect the inability of one base pair to restore the normal helical state after the junction. Another possibility is that the hydrophobic hydration may be removed before melting of the hairpins. The T_M of the hairpins is much higher than that of the duplexes due to their intramolecular character and higher GC content. Thus, the unfolding of the hairpins takes place at higher temperatures and is accompanied by a reduced hydrophobic hydration.

Thermodynamic Release of Counterions. As expected, the resulting Δn_{Na^+} parameters are lower than the Δn_{Na^+} of 0.17 mol of Na^+ per phosphate of a nucleic acid polymer (*35*). This is consistent with previous results and reflects their size difference and end effects (*36*, *37*). Moreover, the hairpins have a smaller release of counterions than the duplexes due to differences in their transition molecularity and the presence of Coulombic end effects, which increase with decreasing oligomer length (*36*). Therefore, appropriate comparisons between Okazaki fragments and control molecules can be done only within the molecules in each set. On the basis of their Δn_{Na^+} values, we conclude that the DNA and RNA duplexes have similar charge densities, whereas the hybrid duplexes exhibit smaller charge densities. The smaller interstrand phosphate distance of the B conformation is compensated by its larger intrastrand phosphate distance, resulting in a similar charge density for the A and B conformations. The mixed conformation of the hybrid duplexes may not allow the compensation of intra- and interstrand phosphate distances, resulting in duplexes with a smaller charge density. The DNA duplexes containing uridine bases exhibit a smaller release of counterions compared to the nonsubstituted DNA. This decrease is consistent with the observed decrease in stacking interactions, which results in a larger separation of the intrastrand phosphates and a smaller charge density parameter. The charge density of OKA is between those of its component DNA and hybrid segments. The coexistence of hybrid segment and a DNA segment changes the direction of the helical axis, which results in a helical bend (*5*, *7*). The presence of this bend in OKA may result in closer proximity of the phosphates around the junction. However, the contribution of the junction to the charge density of the overall structure may be small, resulting in a counterion release that is between that of the DNA and hybrid duplexes. In the case of the hairpins, the contribution of the junction to the overall structure is larger and results in a higher charge density of OKA-hp relative to U-loop.

Binding Profiles for the Interaction of Intercalators with Hairpins. U-loop and OKA-hp contain one binding site for EB and PI in the middle of the stem of these hairpins. In the case of OKA-hp this site is at the DNA−RNA junction. The interaction of EB (and PI) with OKA-hp exhibits a −3.5 kcal/mol (−2.0 kcal/mol) more exothermic heat than with U-loop and −2.9 kcal/mol (−0.5 kcal/mol) with a similar hairpin containing thymine loops (*19*, *23*). These favorable enthalpy contributions may be explained in terms of a structural dehydration event and/or a higher exposure of the aromatic bases at the RNA−DNA junction, resulting in a larger surface contact with the phenanthroline ring of the intercalators and an increased binding affinity, if the entropy contributions are similar. However, EB binding affinities are 1 order of magnitude greater for U-loop (and T-loop) than for OKA-hp, whereas the PI binding affinities have similar magnitudes with all three hairpins, as shown in Table 2. The decreased binding affinity of EB reflects an unfavorable entropy contribution, which in the case of PI (with an extra charge) is compensated by the additional electrostricted dehydration of the ligand and favorable electrostatic contributions. This unfavorable entropy contribution may arise from intercalator binding to the stem of OKA-hp, which optimizes stacking interactions around the flexible flanking bases of the RNA−DNA junction.

Chart 2: Structures of Intercalators

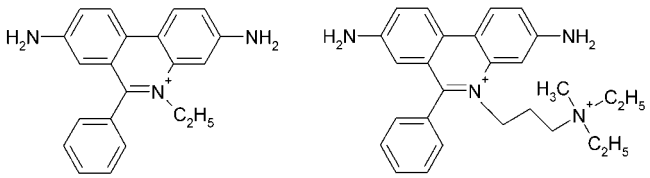

Ethidium Propidium

The resulting stoichiometries in excess of one ligand per hairpin reflect additional binding sites in the loops, which is consistent with previous investigations with T-loop. Table 2 indicates that EB and PI bind the loops of these hairpins with similar affinities of $\sim 5 \times 10^5$. One EB molecule binds the loop of OKA-hp and two bind the loop of U-loop and T-loop, whereas two PI molecules bind the loops of all three hairpins. This indicates that the structural distortions induced by the RNA−DNA junction can gradually propagate over the constrained uridines of the loop of OKA-hp. This loop may have a conformation different from that of the other loops in terms of base−base stacking interactions. The interaction of PI with the stem of OKA-hp is stronger than that of EB and, therefore, it is reasonable to speculate that the induced perturbations, unwinding and unstacking, of this intercalator reorient the loops for ligand binding more effectively than EB.

In general, the interactions of either hairpin with PI are less exothermic than the interactions of EB, consistent with previous observations (*38*). We can dissect their binding enthalpy into two contributions: an exothermic contribution due to stacking interactions of the phenanthroline ring and the aromatic DNA bases, and an endothermic contribution due to a release of water molecules upon binding of the intercalator. As both dyes have similar phenanthroline rings, the contributions of stacking interactions should be similar for both dyes. The release of water reflects the dehydration of both DNA and dye. The structures of EB and PI are shown in Chart 2. The main difference is that one H in EB is replaced by a bulky and charged quaternary ammonium group in PI. Thus, the lower binding enthalpies of PI probably reflect a differential dehydration effect of the ligands due to the presence of the extra charge of PI, which results primarily in endothermic contributions due to the release of electrostricted water from the DNA and the ligand.

CONCLUSION

We used a combination of spectroscopic and calorimetric techniques to determine complete thermodynamic profiles accompanying the folding of a model Okazaki fragment and its control DNA, RNA, and hybrid duplexes. The CD spectra indicate that this fragment adopts an intermediate A−B conformation. Standard thermodynamic profiles show that the stability of this fragment is between those of the DNA and RNA duplexes and is higher than expected from its overall composition, 50% DNA and 50% DNA/RNA hybrid. From an energetic point of view, this hierarchy may be of biological significance because it may allow the appropriate removal of the RNA fragment after cleavage of the RNA−DNA junction. The Δn_{Na^+} parameter indicated that Okazaki fragments exhibit charged densities between those of their component DNA and hybrid sequences consistent with its mixed conformation and overall electrostatic contributions. The overall ranking of the thermodynamic parameters is interpreted in terms of the presence of an RNA−DNA junction. This junction confers Okazaki fragments with stabilities higher than expected based on their component DNA and hybrid segments. Moreover, the phenanthroline ring of the intercalators makes a larger surface contact with the bases at the RNA−DNA junction, resulting in a larger disruption of the flexible flanking bases of the junction. Our overall results suggest that the presence of an RNA−DNA junction stabilizes Okazaki fragments and provides a structural feature that can be exploited in the design of intercalators that specifically target Okazaki fragments. Moreover, the presence of an RNA−DNA junction can be used to modify the binding affinity of model drugs for a particular sequence. This suggests that Okazaki fragments and their unique structural features may have contributed to the evolution of RNase H to optimize recognition and cleavage of the RNA primers during lagging strand processing.

ACKNOWLEDGMENT

The editorial help of Susan Fienhold is greatly appreciated.

REFERENCES

1. Okawa, T., and Okazaki, T. (1980) *Annu. Rev. Biochem. 49*, 421−457.
2. Gmeiner, W. H., Skradis, A., Pon, R. T., and Liu, J. (1998) *Nucleic Acids Res. 26*, 2359−2365.
3. Gmeiner, W. H. (1998) *Curr. Med. Chem. 5*, 115−135.
4. Murante, R. S., Henricksen, L. A., and Bambara, R. A. (1998) *Proc. Natl. Acad. Sci. U.S.A. 95*, 2244−2249.
5. Selsing, E., Wells, R. D., Alden, C. J., and Arnott, S. (1979) *J. Biol. Chem. 254*, 5417−5422.
6. Gmeiner, W. H., Konerding, D., and James, T. L. (1999) *Biochemistry 38*, 1166−1175.
7. Salazar, M., Fedoroff, O. Y., and Reid, B. R. (1996) *Biochemistry 35*, 8126−8135.
8. Fedoroff, O. Y., Salazar, M., and Reid, B. R. (1996) *Biochemistry 35*, 11070−11080.
9. Gmeiner, W. H., Cui, W., Konerding, D. E., Keifer, P. A., Sharma, S. K., Soto, A. M., Marky, L. A., and Lown, J. W. (1999) *J. Biomol. Struct. Dyn. 17*, 507−518.
10. Gmeiner, W. H., Cui, W., Sharma, S. K., Soto, A. M., Marky, L. A., and Lown, J. W. (2000) *Nucleosides, Nucleotides Nucleic Acids 19*, 1365−1379.
11. Cantor, C. R., Warshaw, M. M., and Shapiro, H. (1970) *Biopolymers 9*, 1059−1077.
12. Marky, L. A., Blumenfeld, K. S., Kozlowski, S., and Breslauer, K. J. (1983) *Biopolymers 22*, 1247−1257.
13. Bresloff, J. L., and Crothers, D. M. (1975) *J. Mol. Biol. 95*, 103−123.
14. Patel, D. J., and Canuel, L. L. (1977) *Proc. Natl. Acad. Sci. U.S.A. 74*, 2624−2628.
15. Marky, L. A., and Breslauer, K. J. (1987) *Biopolymers 26*, 1601−1620.
16. Hall, K. B., and McLaughlin, L. W. (1991) *Biochemistry 30*, 10606−10613.
17. Ratmeyer, L., Vinayak, R., Zhong, Y. Y., Zon, G., and Wilson, W. D. (1994) *Biochemistry 33*, 5298−5304.
18. Rentzeperis, D., Kharakoz, D. P., and Marky, L. A. (1991) *Biochemistry 30*, 6276−6283.
19. Rentzeperis, D., Alessi, K., and Marky, L. A. (1993) *Nucleic Acids Res. 21*, 2638−2689.
20. Deppert, W., and Schirmbeck, R. (1995) *Int. Rev. Cytol. 162A*, 485−537.
21. Turchi, J. J., Huang, L., Murante, R., Kim, Y., and Bambara, R. A. (1994) *Proc. Natl. Acad. Sci. U.S.A. 91*, 9803−9807.
22. Konerding, D., James, T. L., Trump, E., Soto, A. M., Marky, L. A., and Gmeiner, W. H. (2002) *Biochemistry 41*, 839−846.
23. Rentzeperis, D., Medero, M., and Marky, L. A. (1995) *Bioorg. Med. Chem. 3*, 751−759.
24. Krugh, T. R., and Reinhardt, G. C. (1975) *J. Mol. Biol. 97*, 133−162.
25. Salazar, M., Fedoroff, O. Y., Miller, J. M., Ribeiro, S. N., and Reid, B. R. (1993) *Biochemistry 32*, 4207−4215.
26. Salazar, M., Champoux, J. J., and Reid, B. R. (1993) *Biochemistry 32*, 739−744.
27. Gyi, J. I., Conn, G. L., Lane, A. N., and Brown, T. (1996) *Biochemistry 35*, 12538−12548.
28. Lane, A. N., Ebel, S., and Brown, T. (1993) *Eur. J. Biochem. 215*, 297−306.
29. Selsing, E., Wells, R. D., Early, T. A., and Kearns, D. R. (1978) *Nature 275*, 249−250.
30. Saenger, W. (1984) *Principles of Nucleic Acid Structure* (C. R. Cantor, Ed.), Springer-Verlag, New York.
31. Marky, L. A., and Kupke, D. W. (2000) *Methods Enzymol. 323*, 419−441.
32. Marky, L. A., Rentzeperis, D., Luneva, N. P., Cosman, M., Geancintov, N. E., and Kupke, D. W. (1996) *J. Am. Chem. Soc. 118*, 3804−3810.
33. Kankia, B. I., Kupke, D. W., and Marky, L. A. (2001) *J. Phys. Chem. B 105*, 11402−11405.
34. Alessi, K. (1995) Ph.D. Dissertation, New York University, New York.
35. Cantor, C. R., and Schimmel, P. R. (1980) *Biophysical Chemistry*, W. H. Freeman and Co., New York.
36. Olmsted, M. C., Anderson, C. F., and Record, M. T., Jr. (1991) *Biopolymers 31*, 1593−1604.
37. Record, M. T., Jr., and Lohman, T. M. (1978) *Biopolymers 17*, 159−166.
38. Marky, L. A., Macgregor, R. B., Jr. (1990) *Biochemistry 29*, 4805−4811.

BI025715O